Oil & Gas Science and Technology – Rev. IFP, Vol. 60 (2005), No. 1, pp. 193-206

IFP International Workshop
Rencontres scientifiques de l'IFP

Gas-Water-Rock Interactions ... / Interactions gaz-eau-roche ...

A New Experimental Procedure for Simulation of H_2S + CO_2 Geological Storage

Application to Well Cement Aging

N. Jacquemet[1], J. Pironon[1] and E. Caroli[2]

1 UMR CNRS 7566 G2R et CREGU, UHP, BP 239, 54506 Vandœuvre-lès-Nancy Cedex - France
2 CSTJF, Total, avenue Larribau, 64018 Pau Cedex - France
e-mail: nicolas.jacquemet@g2r.uhp-nancy.fr - jacques.pironon@g2r.uhp-nancy.fr - emmanuel.caroli@total.com

Résumé — Nouvelle procédure expérimentale destinée à la simulation d'une séquestration géologique de H_2S + CO_2. Application au vieillissement des ciments de puits — Nous proposons une nouvelle procédure expérimentale destinée à étudier la réactivité des systèmes H_2S + CO_2-saumure-solides dans des conditions de haute pression et haute température (jusqu'à 990 bar et 450 °C). Un montage sous la forme d'une ligne de gaz a été conçu afin d'introduire de façon précise une quantité de gaz dans des microréacteurs. Des systèmes à très forte concentration en gaz peuvent être étudiés dans le respect des règles de sécurité. Nous avons adapté la technique des inclusions fluides synthétiques à cette procédure. Cette technique permet l'échantillonage *in situ* des fluides pendant les expérimentations. Les bilans de masse des espèces gazeuses permettent de quantifier leur consommation ou leur genèse. Les résultats de deux vieillissements de ciment de puits, d'une part en présence de saumure (expérimentation 1), et d'autre part en présence de saumure et de H_2S + CO_2 (expérimentation 2), sont présentés en tant qu'application de cette procédure expérimentale. Les conditions choisies furent 500 bar, 200 °C pour une durée de 15 jours. Dans un environnement constitué par une saumure (expérimentation 1), le ciment initialement composé d'un assemblage de tobermorite (CSH) est converti en un assemblage de xonotlite (CSH). Cette transformation s'est effectuée dans une gamme de pH de l'ordre de 10.3-11.2. La présence d'H_2S et CO_2 (expérimentation 2) provoque une chute de pH (de 10.3-11.2 à 8-9) et de Eh (de conditions oxydantes à des conditions réductrices). Ces conditions ont conduit à une carbonatation partielle du ciment et à la transformation des phases porteuses de fer (Fe° de l'acier et C_4AF du ciment) en pyrite (FeS_2). Le ciment a ainsi été transformé en un assemblage de tobermorite décalcifiée et de calcite ($CaCO_3$). En outre, la procédure utilisée nous a permis d'estimer les consommations molaires de H_2S et CO_2 aux valeurs respectives de 6 et 16%. La consommation de H_2S est essentiellement due à sa combinaison avec le Fe° de l'acier pour former des sulfures. La valeur de la consommation de CO_2 permet d'estimer que le ciment vieilli est composé de 5 volumes de tobermorite contre 1 volume de calcite. Les observations effectuées au microscope électronique à balayage sont en accord avec cet ordre de grandeur.

Abstract — ***A New Experimental Procedure for Simulation of H_2S + CO_2 Geological Storage. Application to Well Cement Aging*** — *We propose a new experimental procedure to study reactivity of H_2S+CO_2-brine-solid systems under high pressure and temperature conditions (up to 990 bar and 450°C). A gas loading device has been made in order to fill accurately microreactors with absolute quantity of gaseous reactants. High gas concentrations can also be reached securely. The technique of synthetic fluid inclusions has been adapted to this procedure. This technique provides an* in situ *sampling*

of fluids during experiments. After experiments, mass balance of gaseous species can be calculated and thus the molar consumption/genesis percentage. Results of well cement aging in the presence of brine (experiment 1) and in the presence of brine plus H_2S + CO_2 (experiment 2) are presented as an example of application of this procedure for the simulation of gas storage. The conditions of the two experiments were 500 bar, 200°C, 15 days. In brine environment (experiment 1), the cement is converted from an assemblage of tobermorite (CSH) to an assemblage of xonotlite (CSH). This transformation occurred in a pH range of 10.3-11.2. The presence of H_2S-CO_2 mixture (experiment 2) induces pH (from 10.3-11.2 to 8-9) and Eh (from oxidising conditions to reductive conditions) decreases. These conditions lead to the partial cement carbonation and to the sulphidation of iron bearing phases (steel and C_4AF). In this case, the cement was transformed to an assemblage of slight Ca-depleted tobermorite plus calcite. The procedure allowed also to determine an H_2S and CO_2 molar consumption respectively of 6 and 16%. The H_2S consumption is essentially related to the sulphidation of steel. The CO_2 consumption predicts a reacted cement composed of 5 volumes of tobermorite for 1 volume of calcite. This estimation is coherent with the scanning electron microscope observations.

INTRODUCTION

Sour natural gas contains undesirable components: hydrogen sulfide (H_2S) and carbon dioxide (CO_2). Industrial processes permit sulphur recovery from H_2S but such operations can be uneconomical and the sulphur market is saturated (Wichert, 1996; Wichert, 1997; Chakma, 1997; Carroll and Maddocks, 1999). Sulphur compound flaring restrictions prevent the release of H_2S in air (Chakma, 1997; Carroll and Maddocks, 1999; Connock, 2001). It is generally agreed that increasing amount of CO_2 in atmosphere contribute to global climate warming (IPCC, 2001). Thus, CO_2 discharging will soon be regulated too. Consequently, the petroleum industry has to develop alternative ways for acid gas elimination. Reinjection into geological reservoirs (*i.e.* deep saline aquifers in western Canada and depleted oil and gas reservoirs) seems to be one of the most often considered solutions for acid gas release mitigation (Reichle *et al.*, 1999; Bachu, 2000; Davison *et al.*, 2001; Reeve, 2001; Bachu, 2002; Bruant *et al.*, 2002; Feugier, 2002). There are currently about 30 operating H_2S + CO_2 reinjections into both depleted oil and gas reservoirs and aquifers (Chakma, 1997; Wichert, 1997; Connock, 2001). Injected mixtures contain 5 to 75% of H_2S (Wichert, 1997). Sulphur burden is thereby reduced and risks associated with his handling are also reduced. CO_2 emission is avoided too. This solution could permit development of sour gas reservoirs located in Canada, Venezuela, Middle East and Caspian basin which constitute one third of natural gas reserves.

Interactions between H_2S+CO_2 fluid and minerals are likely to occur during and after the injection stage both in reservoirs and at the well-reservoir interface. Interactions between gas, formation water, hydrocarbons, host rock minerals and well materials (*i.e.* cement and steel) could modify porosity and permeability of the reservoir and affect the integrity of cement and steel providing pathways for leaks (Chakma, 1997; Reichle *et al.*, 1999; Bruant *et al.*, 2002; Celia and Bachu, 2002). Environmental and human impacts make them an issue for acid gas geological storage (Davison *et al.*, 2001; Bruant *et al.*, 2002). In addition, interactions between H_2S+CO_2 fluid and minerals can result in the gas solubilisation and/or mineralisation. The latest mechanisms are the main ways to trap acid gases. Thus, the study of interactions are essential to define the trapping efficiency of reservoirs.

Both numerical modelling and experimental investigations had been conducted to study such systems. Experimental approaches to study reactivity of host-rocks minerals were presented by Pearce *et al.* (1996), Gunter *et al.* (1997), Shiraki and Dunn (2000), Giammar *et al.* (2002), Kaszuba *et al.* (2003), Soong *et al.* (2004). Well cements durability in presence of CO_2 at high P-T was examined by Onan (1984), Shen (1989), Krilov *et al.* (2000). Corrosion behaviour of tubing steel under super-critical CO_2 conditions was studied by Cui *et al.* (2004) and corrosion of steel under wet H_2S environment is well documented (Cieslak *et al.*, 1998; Albarran *et al.*, 1999; Domizzi *et al.*, 2001; Carneiro *et al.*, 2003). The maximal P-T conditions of the experiments related to sequestration were 200 bar and 200°C for Kaszuba *et al.* (2003) and 300 bar and 180°C for Krilov *et al.* (2000). These conditions do not represent deep geological conditions since the range of reservoir P-T conditions is wide, approximately 50-200°C and 20-1000 bar (Kaszuba *et al.*, 2003). Further, none of the references cited above deals with fluid-minerals systems containing significant quantities of H_2S. This paper presents a new experimental procedure for studying highly H_2S + CO_2 concentrated systems at high P-T conditions. As an example of application, a well cement aging study in such harsh environment is presented.

1 EXPERIMENTAL PROCEDURE

1.1 Reactors

Experiments are conducted in batch type reactors. They are constituted by flexible sealed gold capsules. Gold is chemically inert, easily malleable and good heat conductor. So it

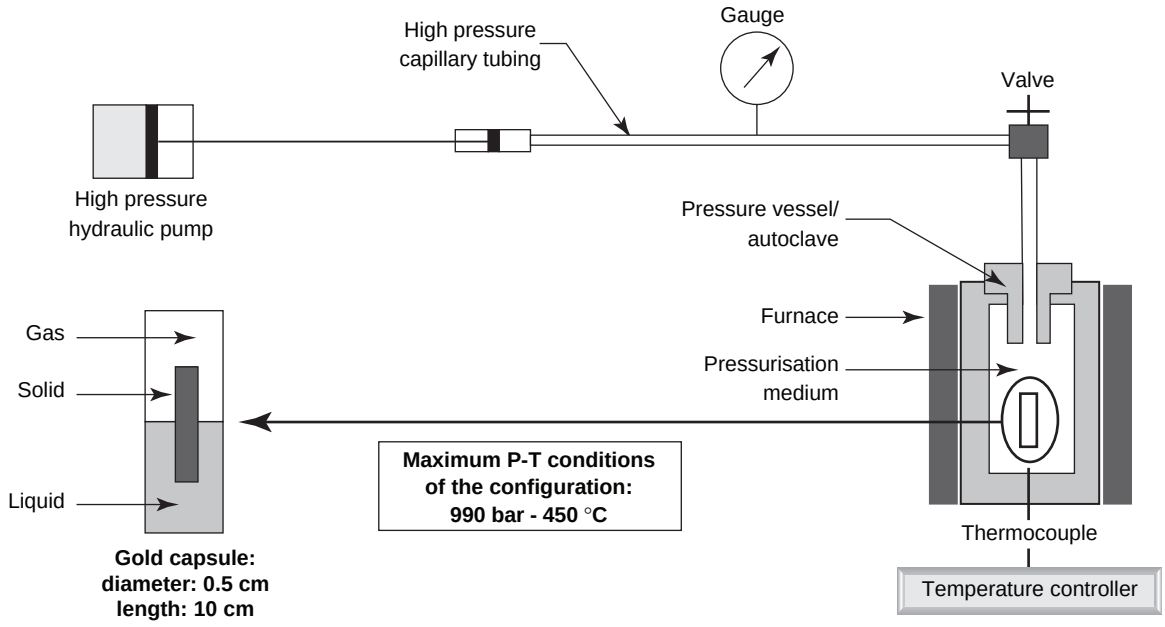

Figure 1

Schematic illustration of the high pressure and temperature configuration. Modified from Teinturier (2002).

does not influence the investigated system and it permits a good transmission of total pressure and temperature (Seyfried *et al*., 1987). Volumes about 2 cm^3 are used to limit the risk linked to H_2S toxicity. In such volumes high H_2S concentrations can be reached safely. Capsules containing reactants are introduced into 100 cm^3 hydraulic pressure vessels manufactured by *Autoclave Engineer* (division of *Snap-tite Inc*.). The autoclave is pressurised and heated by a configuration which permits high P-T conditions (990 bar-450°C) *(Fig. 1)*. The pressurisation medium is a water-oil mixture pressurised by a high-pressure hydraulic pump. A pressure gauge is employed for the control and the measurement of pressure. The autoclave is placed in a regulated furnace. A thermocouple is used to control the temperature in the vicinity of capsules. This configuration is close to the flexible-cell system of Seyfried *et al*. (1987) and has been routinely employed for experimental studies of oil maturation (Landais *et al*., 1989; Teinturier *et al*., 2003) and thermodynamics of complex fluids (Teinturier and Pironon, 2003). We used the technique of synthetic fluid inclusions to provide samples of fluids as the reactors are closed during experiments. This original technique is described below.

1.2 Gas Loading and Collecting

1.2.1 Description of Apparatus

Capsule loading is a two step operation. Solids (*e.g.* reservoir minerals or well material) and liquids (*e.g.* brine) of interest are introduced first into the capsules. The second step is gas loading. This requires an apparatus inspired by the work of Frantz *et al*. (1989) and Lamb *et al*. (1996). It was designed to load safely a known quantity of H_2S + CO_2 into the capsules and to collect and analyse gaseous products after experiments *(Fig. 2)*. This device is mainly made of stainless steel (SS-316) tubing, valves and fittings. Flexible Teflon™ PFA tubing is also used. The gas line-capsule connector is supplied by *Depth of the Earth*. The piercing chamber and gas cell are also made of stainless steel. All components of this system are compatible with dry and wet H_2S (Clavel *et al*., 1997).

This apparatus is composed of three parts *(Fig. 2)*:

– a gas inlet;
– a calibrated capacity of variable volume and connected to a pressure transducer;
– a gold capsule ending.

Additional valves (E and F) permit connections to the piercing chamber and the gas cell. They are used to collect and analyse gaseous products after experiments.

H_2S is toxic and flammable, thus its manipulation requires great care. The gas cylinder is placed outside the laboratory. A low pressure (2 bar) gas line carries the gas to the loading local, which is well ventilated and equipped with H_2S sensors. Gas handling is performed under a laboratory hood with a bottom gas extraction. *Bureau Veritas* provided the conformity assessment for H_2S manipulation.

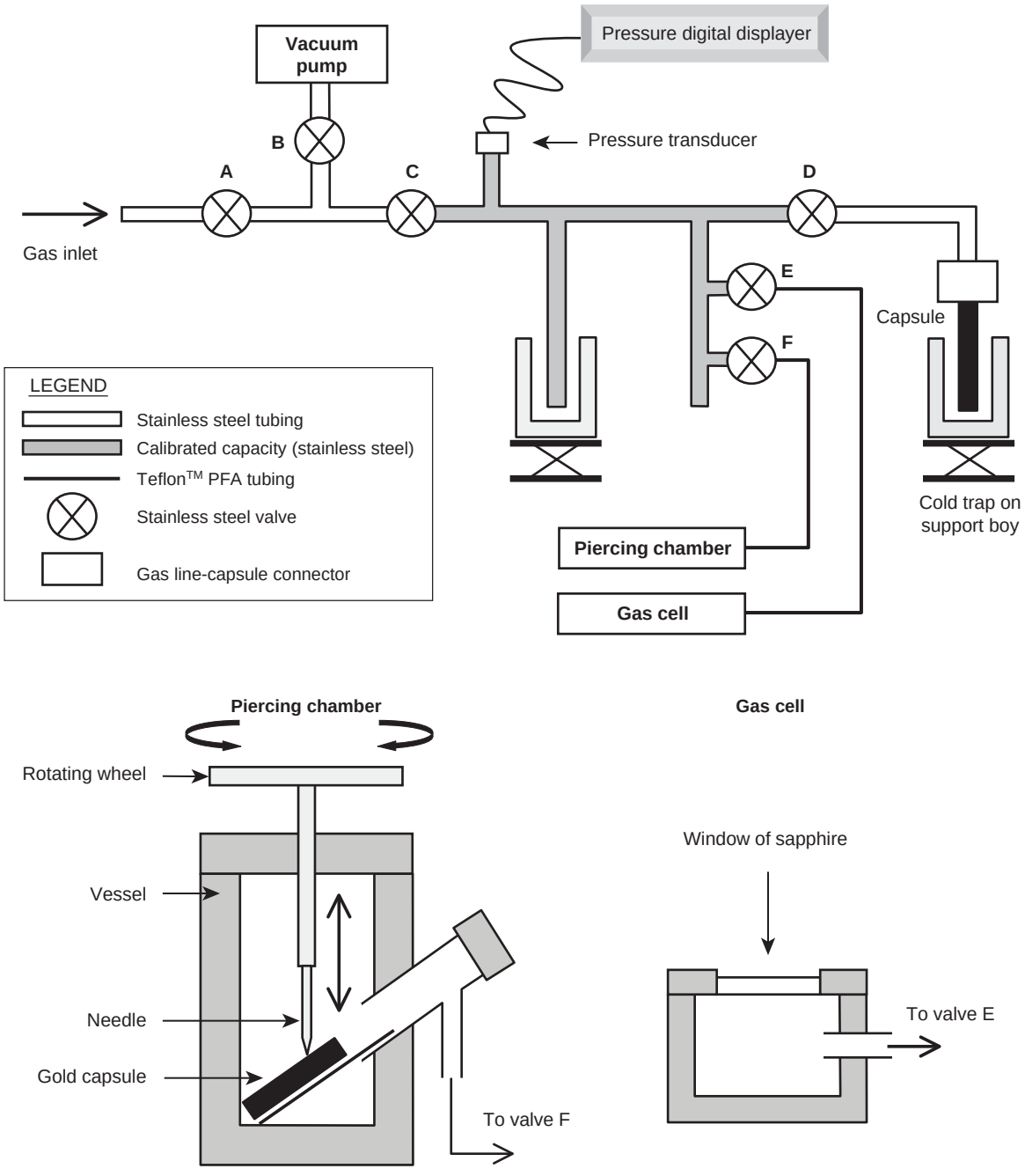

Figure 2

Schematic illustration of the gas loading and collecting apparatus. Modified from Frantz *et al.* (1989) and Lamb *et al.* (1996).

1.2.2 Gas Loading Procedure

The piercing chamber and the gas cell are disconnected and valve E, F and B are closed while C is open *(Fig. 2)*. To prevent air contamination during admission of gas in the apparatus, one makes a gas flow through the line by opening valve A. After 1 min, this valve and valve D are closed. The capsule containing solid and liquid reactants is then fitted to the apparatus with the gas line-capsule connector. The capsule is partly immersed in a liquid nitrogen bath to freeze and hold liquid(s) and solid(s) reactants into the capsule during pumping. After the opening of valves B, C and D the vacuum pump is switched on to evacuate residual gas until reaching pressure lower than 0.01 bar while the capsule still cools. Valves D and B are then closed. By opening valve A, the gas mixture is allowed to penetrate into the calibrated capacity. By opening the valve D (valve A closed), the quantity of gas contained in the calibrated capacity is transferred by cold trapping (cryocondensation) into the cooled capsule. The capsule is then sealed using a pinch-off device (crimping plier) and removed from the gas line. The capsule is then welded while it remains in the liquid nitrogen bath and plunged into water to control the welding efficiency by the absence of leakage.

On of the interests of this device is the control of the absolute gas quantity enclosed in the capsule. It is thus possible to vary the concentration of gas into the system. The required quantity of gas (n_{req}) can be expressed as a pressure *(EP)* for a calibrated capacity of volume V via the Equation (1) (ideal gas law):

$$n_{req} = \frac{EP \times V}{R \times T} \tag{1}$$

$$R = 8.314 \text{ J·mol}^{-1}\text{·k}^{-1}$$

$$T = 288°\text{K (15°C, ambient temperature)}$$

Thus, the operation of gas loading consists of the enclosure of the pressure EP in the capsule. Different calibrated capacities can be used depending on the amplitude of n_{req}. The pressure of gas contained in the calibrated capacity before cold trapping is called initial pressure *(IP)*. During the stage of cryocondensation, the pressure decreases to a minimum value called final pressure *(FP)*. The FP value depends on the length of capsule plunged into the Dewar flask containing liquid nitrogen. This length is adjusted by a support boy holding the dewar *(Fig. 2)*. The difference IP-FP is equal to EP. After sealing and welding, the final mass of the capsule is determined by weighing. The difference between the final mass of the capsule and its mass before gas loading gives the real total quantity of gas enclosed in the capsule $(n1_T)$. The relative difference between the $n1_T$ and n_{req} for 12 loading operations ranges from 3 to 9%. The loading operation allows thus an accurate control of the gas concentration of the system. The molar ratios of each gas species i $(X1_i)$ in the initial gas mixture are known. Multiplying these molar ratios with $n1_T$ gives the number of mole for each species i contained in the system before experiment $(n1_i)$.

The molar compositions of the initial gas mixture (before loading) and of the gas from a capsule just after crycondensation are similar *(Table 1)*. The cold trapping does not modify the composition of the initial gas mixture. There is no preferential condensation of one species relative to the other during cryocondensation. The cold trapping can be thus used for the loading of different gas mixtures in which triple point temperature of each constituent is higher than the liquid nitrogen temperature (–195°C).

TABLE 1

Molar composition of the initial gas mixture, of the gas after cryocondensation and of the residual gas after experiment 2. The compositions are determined by Raman spectroscopy

	H_2S (% mol)	CO_2 (% mol)
Initial gas	66	34
Gas after loading stage (cryocondensation)	66.3	33.7
Residual gas after experiment 2	68.4	31.6

1.2.3 Gas Collecting Procedure

After experiments, each gold capsule is removed from the autoclave and placed in the piercing chamber connected to the apparatus. The volume comprising the volume of the chosen calibrated capacity plus the volume of the piercing chamber is called V'. After vacuum, the capsule is pierced. The gaseous product is released into the volume V' and the pressure is read on the digital display and called the residual pressure *(RP)*. Thus, the total quantity of gas contained in the system after experiment $(n2_T)$ can be expressed as:

$$n2_T = \frac{RP \times V'}{R \times T} \tag{2}$$

If the value $(n2_T - n1_T)$ is greater than 0, gas was consumed by the reactions whereas if $(n2_T - n1_T)$ is lower than 0, gas was generated by the reactions. The molar rate of total gas consumption (GC_T) or genesis (GG_T) during experiments can be expressed as follows:

$$GC_T = \frac{(n1_T - n2_T)}{n1_T} \times 100 \tag{3}$$

$$GG_T = \frac{(n2_T - n1_T)}{n1_T} \times 100 \tag{4}$$

The Raman analysis of residual gas described below gives the molar ratios of each gas species i $(X2_i)$. Multiplying $X2_i$

by $n2_T$ gives the residual number of mole for each species ($n2_i$). The molar percentage of gas consumption *(GC_i)* or genesis *(GG_i)* for each species is then given by the Equations (5) and (6):

$$GC_i = \frac{(n1_i - n2_i)}{n1_i} \times 100 \quad (5)$$

$$GG_i = \frac{(n2_i - n1_i)}{n1_i} \times 100 \quad (6)$$

1.3 Analysis Protocol

1.3.1 Fluids

Residual Gas

The finger of the calibrated capacity is cooled to condense gaseous product while the valve F remains open *(Fig. 2)*. The valve F is then closed and the valve E is open. The gas sublimates to reach a pressure higher than 3 bar in the gas cell. Such minimal pressure is required for accurate Raman analyses. The gas cell has a transparent sapphire window for backscattering Raman analysis *(Fig. 2)*. The Raman microprobe is a Labram type (*Jobin-Yvon*) with a *Notch* filter and a CCD detector cooled at –30°C. The exciting radiation at 514.532 nm is provided by an Ar^+ laser (type 2020, *Spectraphysics*). Two gratings of 600 and 1800 grooves per mm were chosen to combine good spectral resolution and convenient spectral window. The spectral resolution is around 2 cm^{-1} for the 1800 grating used for quantification. The Raman spectra were collected between 100 and 5000 cm^{-1} to detect and quantify gases in the gas cell. This technique allows detection of CO_2 at 1285 and 1388 cm^{-1}, O_2 at 1555 cm^{-1}, CO at 2143 cm^{-1}, H_2S around 2600 cm^{-1}, CH_4 around 2910 cm^{-1} and H_2 at 4156 cm^{-1} (Dubessy *et al*., 1989).

Liquids

After capsule removal from pressure vessels and piercing stage, if there is sufficiently residual liquid in capsule, it is collected in argon (Ar) atmosphere in order to avoid atmospheric CO_2 and O_2 contamination. It is analysed by ionic chromatography to determine the anions concentrations and by ICP-MS/AES (ion coupled plasma mass spectrometry/ atomic emission spectroscopy) to determine the cations.

Synthetic Fluid Inclusions

The characterisation of gaseous or liquid compounds reacting with solid(s) requires sampling of fluids at high P-T conditions. This procedure is complex and dangerous in the case of toxic gases. Sampling of fluid can greatly modify the water-rock ratio and thus the reaction rates. The analysis of the residual fluid at the end of the experiment is affected by reequilibration that occurs at cooling even in the case of rapid quenching. Thus, residual fluid data does not represent accurately pressure-volume-temperature-composition (PVTX) properties of complex fluids present at experiment conditions. For this reason, fluid inclusions are synthesised during the experiment providing an original in situ fluid sampling. The advantage of this technique is the possibility to trap fluids at the maximum P-T conditions of the experiment and to preserve the fluid from atmospheric interactions. The interest of this procedure is also the possibility to analyse fluids under the experiment conditions. This technique has been largely employed for solubility, PVT, critical and phase equilibrium properties studies (Bodnar and Sterner, 1987; Frantz *et al*., 1989; Frantz *et al*., 1992; Lamb *et al*., 1996; Dubessy *et al*., 2001; Lamb *et al*., 2002; Guillaume *et al*., 2003). An example of synthetic inclusions study in the gas-water-salt-oil system is also given by Teinturier *et al*., (2003).

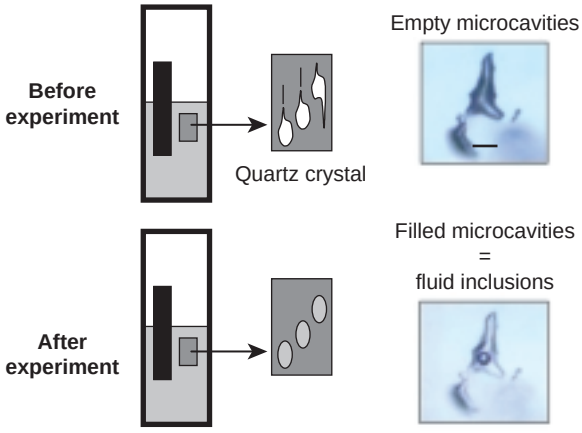

Figure 3

Schematic illustration of fluid trapping into fluid inclusions. Scale bar length is 100 µm.

Microfractured quartz crystals containing empty microcavities are adding to reactants in gold capsules. During an experiment, small quantities of fluids are trapped in these microcavities via a crack network. Then, sealing occurs by quartz precipitation providing closed fluid inclusions *(Fig. 3)*. In the case of geological gas storage, quartz is already present in cement, reservoir or cap-rocks. Thus, the presence of quartz used as a trapping agent does not affect the reactivity of the system. More, the trapped fluid is assumed to be in equilibrium with quartz. Thus, reactions after inclusions sealing are not apt to occur. After the experiments, the quartz crystals are removed from capsules and polished. First observations by optical microscopy can reveal possible immiscibility marked by the presence of different coexisting fluid phases (L+V, L_1+L_2, L_1+L_2+V) at 25°C. Then, microthermometry and Raman microspectroscopy analyses are done. Microthermometric measurements were obtained using a *Linkam* heating and freezing stage adapted to an *Olympus*

microscope equipped with × 50 and × 80 long working distance objectives. This equipment permits the optical detection of phase transition inside fluid inclusions from the temperature of liquid nitrogen (–195°C) up to 600°C. The melting and eutectic temperatures give indications of the ionic nature and concentration, whereas homogenisation temperatures correspond to the intersect of the isochore and the bubble point curve of the brine-gas system. The nature of the phases and the quantification of gaseous and aqueous species are provided by Raman microspectrometry. In the spectra, the broad band corresponding to the stretching vibrations of water is between 3000 and 3500 cm^{-1}. The chlorinity of the solution can be also determined by the water band shape analysis (Dubessy *et al*., 2002). Raman molecular spectroscopy is well adapted for the speciation determination. For instance, HS^- is detected at 2574 cm^{-1} or $H_2S_{(aq)}$ detected at 2590 cm^{-1} and HCO_3^- at 1017 cm^{-1}. This technique is thus efficient in determining Eh and/or pH conditions. A *Linkam* stage can be fixed on the microscope of the Raman microprobe to make measurements at variable temperature until the experiment temperature. Microthermometry and Raman microprobe techniques allow us to have indications about the state and composition of phases at the experiment conditions.

1.3.2 Solids

Texture and mineralogy of solids (*e.g.* rocks or well materials) were characterised using optical microscopy, X-ray diffraction (XRD), scanning electron microscopy (SEM) and transmission electron microscopy (TEM). X-ray patterns were recorded on powdered samples at *LEM* laboratory (Nancy, France) using a *Bruker* D8 diffractometer, with Co K_α radiation. Diffractograms were recorded from 2 to 75° 2θ, with a step scan of 0.036° 2θ and time per step of 2 s. Samples analysed with the SEM are broken fragments and polished sections of solids. The first preparation is adequate to determine the solid texture and the second is used to determine and quantify mineralogy. Micrographs and chemical analysis were performed on an *Hitachi* S-2500 (LaB_6) SEM equipped with *Noran* energy dispersive spectrometry (EDS) and back scattered electron (BSE) detector at *Service commun de l'université H.-Poincaré* (Nancy, France). The accelerating potential was dependent on application. TEM provides micro-imaging, electron diffraction and chemical analyses of isolated microparticles up to 10^{-10} m. Thus, it is a powerful technique to obtain information about morphology, crystallography and chemical composition of finely crystallised solids such as cements. We used a CM20 *Philips* instrument operating at 200 kV equipped with Si-Li detector and Li super ultra thin windows SUTW equipped with an *EDAX* energy dispersive X-ray analyser at *Service commun de l'université H.-Poincaré* (Nancy, France). Spectra were collected under nanoprobe mode, during 40 s from an area of around 10 nm in diameter. Elemental composition was calculated with a maximum error of 5% for each element. Sample particles were deposited onto a Cu grid covered by a carbon film after grinding and dispersion in ethanol. After evaporation of ethanol, the grid was then put into the TEM chamber.

2 AN EXAMPLE OF APPLICATION: WELL CEMENT AGING IN BRINE AND IN BRINE + H_2S + CO_2 AT 500 BAR AND 200°C

2.1 Experimental Approach

Two experiments were conducted to identify the effect of acid gas on cement transformation:

- experiment 1: cement (fragment and powder) with steel and brine;
- experiment 2: cement (fragment and powder) with steel, brine, H_2S and CO_2.

Cement as powder (powder fraction) was used to increase solid reaction surface and then to produce maximum rate of reactivity. For the experiment 1, doublets of capsules were filled with reactants and welded under vacuum. The brine to cement mass ratios were about 2.4 and the cement to steel mass ratios were about 3. For the experiment 2, doublets of capsules were filled first with solids and brine. Gas was then loaded using the procedure described above. The gas to brine and the brine to cement mass ratios were 1. The cement to steel mass ratio was 4. Fractured crystals of quartz containing empty microcavities were added in each capsule to produce synthetic fluid inclusions.

The P-T conditions selected for the experiments were 500 bar and 200°C. Duration of experiments was 15 days. The temperature of 200°C is higher than the average temperature of a deep reservoir. It was selected to counterbalance short duration of experiments.

2.2 Materials

Cement and steel were provided by *Total*. Steel is a low-alloyed one (C22E or XC18 type) and typical of oil-well tubing. The brine was a 150 g/l (2.75 molal) NaCl solution. As the salinity of formation waters in usual oilfields ranges between 0 to 400 g/l and Na and Cl are the predominant ions (Gravier, 1986; Jahn *et al*., 1998), one can consider the chosen brine as an intermediate one. The composition of gas was 66% molar H_2S + 34% molar CO_2. This composition is similar to several injected gas mixtures currently operating in western Canada (Chakma, 1997; Wichert, 1997).

The cement was obtained by curing a slurry at 210 bar and 140°C during 8 days in an aqueous media. It is considered as an analogue of a well cement which hardened in deep conditions. The slurry was composed of Portland cement, silica flour (35% by weight of cement) and water (W/C = 0.55). The Portland cement is of class G, type high sulfate

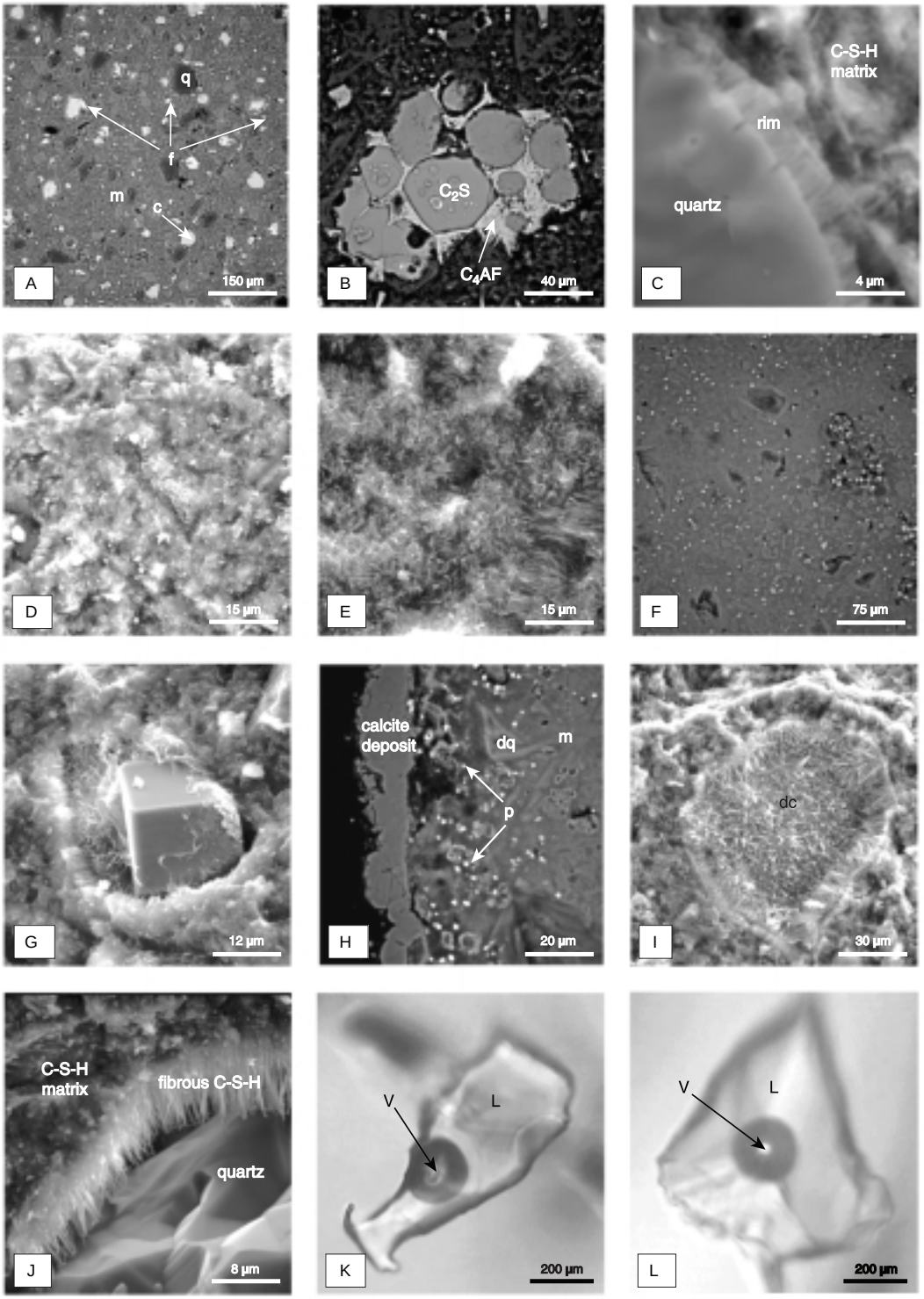

Figure 4

SEM observations of the initial cement (A, B, C and D), the cement of the experiment 1 (E) and the cement of the experiment 2 (F, G, H, I and J). A: polished section observed in BSE mode; B: clinker remnant with appearance of "bunch of grapes" (cluster of C_2S surrounded by C_4AF) observed in BSE mode on polished section; C: quartz corrosion observed on broken fragment; D: matrix observed on broken fragment; E: matrix observed on broken fragment; F: polished section observed in BSE mode, the white minerals are pyrites; G: euhedral pyrite observed on broken fragment; H: calcite crust observed in BSE mode on polished section; I: dissolved C_2S observed on broken fragment; J: dissolved quartz observed on broken fragment. K: fluid inclusion of the experiment 1 at room temperature; L: fluid inclusion of the experiment 2 at room temperature. m: C-S-H matrix; c: C_2S; f: ferrite; q: quartz; dq: dissolved quartz; p: pyrite; dc: dissolved C_2S.

resistant, defined on API specification 1O, similar to the ISO 10426-1 specification, and similar to the ASTM II type (Méducin *et al*., 2001; Méducin *et al*., 2002).

The colour of cement is grey. SEM observations on polished sections showed the cement is essentially composed of a C-S-H matrix and phenocrystals of quartz, C_2S and C_4AF in minor proportions (*Fig. 4, A*). The C_2S and C_4AF are anhydrous remnants of the clinker (*Fig. 4, B*). The quartz phenocrystals compose the silica flour added to the slurry. They were partially corroded by the pouzzolanic reactions that occurred during the cure (*Fig. 4, C*). XRD analysis detected the reflections of quartz and very weak reflections attributed to 11 Å tobermorite *(Fig. 5)*. The composition of the 11 Å tobermorite, also simply called tobermorite (Taylor, 1997) is given by the Table 2. The detected quartz corresponds to the silica flour addition in the slurry. The XRD analysis shows the cement is essentially amorphous or cryptocrystallised and probably have a composition of 11 Å tobermorite. The amorphous appearance of the C-S-H matrix is confirmed by the SEM observations shown in the Figure 4, D. The TEM microanalysis and observations characterised the C-S-H as the major constituent and hydrogarnet related mineral (Hgt1) as a minor constituent. Amorphous fibrous aggregates and crystallised platelets are the main morphologies of the C-S-H *(Table 2*). These C-S-H morphologies are in good accordance with those described by Taylor (1997) for hydrothermal preparations. The quantitative microanalysis of C-S-H by TEM on individual particles shows small amounts of Al. The Si/Ca and Al/Ca atomic ratios range from 0.6 to 1.63 and from 0 to 0.13 respectively. In the Al/Ca *vs* Si/Ca plot of the Figure 6, the composition of the C-S-H lies between the hillebrandite and anomalous tobermorite poles. The anomalous tobermorite is aluminous and contains less Ca than the common tobermorite. Its composition described by Taylor (1997) is exposed in the Table 2. There is no clear relation between the slightly different compositions and the different morphologies. A mean composition of the C-S-H has been calculated from the TEM microanalysis data and is reported in the Table 2. From this mean composition and crystallographic data, the C-S-H composing the cement matrix can be identified with tobermorites, which combined Al (Tob1). This element is supposed to be in substitution of Si (Kalousek, 1957; Taylor, 1997). The pH of a NaCl brine (150 g/l or 2.75 molal) in equilibrium with the starting cement is between 10.3 and 11.2 at room temperature.

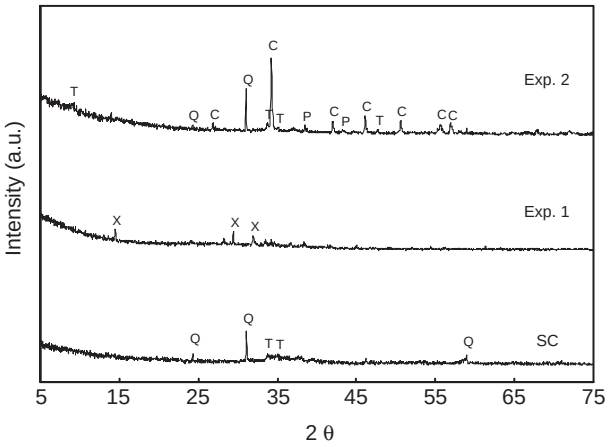

Figure 5

XRD patterns of the starting cement (SC), the altered cement after the experiment 1 (Exp. 1), the altered cement after the experiment 2 (Exp. 2). Q: quartz; X: xonotlite; T: 11 Å tobermorite; C: calcite; P: pyrite.

TABLE 2

C-S-H morphologies and mean compositions deduced from TEM analysis.

Sample	**Morphology**	**Mean composition (% atomic, except O)**			**No. of analyses**
		Si	**Ca**	**Al**	
Starting cement	Amorphous fibrous aggregate, crystallised platelet	48.6	48.1	3.3	21
Experiment 1	Crystallised fibre	49.1	48.5	2.4	6
Experiment 2	Crystallised fibre, crystallised platelet, amorphous fibrous aggregate	57.4	37.5	5.1	16
11 Å tobermorite[1]	Natural: fibrous	52	48	0	
Xonotlite[1]	Natural: fibrous	50	50	0	
Anomalous 11 Å tobermorite[1]		55	40	5	

1 Taylor, 1997.

2.3 Results

The effect of acid gas on cement aging will be checked comparing hydrothermal experiments without (experiment 1) and with H_2S+CO_2 mixture (experiment 2) at 200°C and 500 bar. The solid (cement) and fluid products are characterised after each experiment and compared with the starting reactants. Results about steel corrosion are not presented in this paper.

2.3.1 Experiment 1

Cement

Macroscopic observations showed colour change of the cement. Initially grey, it became pink. White mineral precipitated at its surface and at the surface of the quartz introduced for fluid inclusions trapping. More, dissolution features appeared at the quartz surface. SEM observations on broken fragments revealed a fibrous matrix *(Fig. 4, E)*. XRD analysis on the powder fraction shows the presence of xonotlite and the absence of quartz *(Fig. 5)*. The TEM observations and microanalyses on the powder fraction revealed C-S-H as the major phase and hydrogarnet related minerals (Hgt2) as minor constituents. The C-S-H present an unique morphology of fibre. Their individual microanalyses show a small amount of Al. The Si/Ca and Al/Ca atomic ratios vary from 0.94 to 1.1 and from 0.04 to 0.05 respectively and are reported in the Al/Ca *vs* Si/Ca plot of the Figure 6. The composition seems to be more homogeneous than in the starting cement (SC). This could be related to the unique observed morphology. The mean composition of the C-S-H calculated from the TEM microanalyses is presented in the Table 2. This composition is very similar than that of the starting cement, however crystallography helps us to conclude to the presence of xonotlite which combined Al (Xon) associated to the full dissolution of quartz.

Liquids

No sufficient residual liquid quantity were recovered for analysis. Thus, synthetic fluid inclusions became the only way for fluid investigations. As we mentioned above, the synthetic fluid inclusions provide *in situ* samples of fluid. Only few microcavities in quartz have been sealed producing rare fluid inclusions. At room temperature, the inclusions are diphasic *(Fig. 4, K)*. Each contains an aqueous liquid coexisting with a vapour phase. At 200°C, these inclusions remain diphasic and this anomalous behaviour indicates a fluid leakage from the inclusions. That could be due to a weak sealing evidenced by the important quartz dissolution within the system. Despite this slight leakage, salinity of fluid inclusions can be estimated from the melting temperature of the ice (microthermometry). Raman spectroscopy is also used to determine the chlorinity of the inclusions. 11 inclusions have been analysed by Raman and microthermometry. The values of chlorinity determined by Raman are exposed in the Figure 7. They range from 0.5 to 3.5 molal. These values are different than the chlorinity of the initial brine (2.75 molal). There is a good agreement between the Raman data and the data from microthermometry.

2.3.2 Experiment 2

Cement

No colour change was noticed. SEM observations show occurrence of pyrite (FeS_2) in the pore spaces created by the dissolution of quartz and/or C_2S and within the matrix *(Fig. 4, F* and *G)*. Image analysis on SEM micrographs of polished sections were performed using the software ImageJ (Rasband, 2004). They show that the mean proportion of pyrite can be considered around 2 volume %. A calcite ($CaCO_3$) deposit of at least 15 µm thick has been also observed around the cement fragment by SEM observations *(Fig. 4, H)*. It indicates a diffusion of Ca from the core to the external media. Few crystals of calcite have been observed within the fragment. We also noticed replacement of C_2S by fibrous C-S-H *(Fig. 4, I)* and partially dissolved/replaced quartz by fibrous C-S-H *(Fig. 4, J)*. The XRD analysis on the powder fraction of the cement identified calcite, quartz, 11Å tobermorite and pyrite *(Fig. 5)*. The TEM observations and microanalysis on the powder fraction of the cement revealed the C-S-H as the major phase and calcite and pyrite as minor phases. The C-S-H have a morphology of crystallised fibres, crystallised platelets and amorphous fibrous aggregates. The

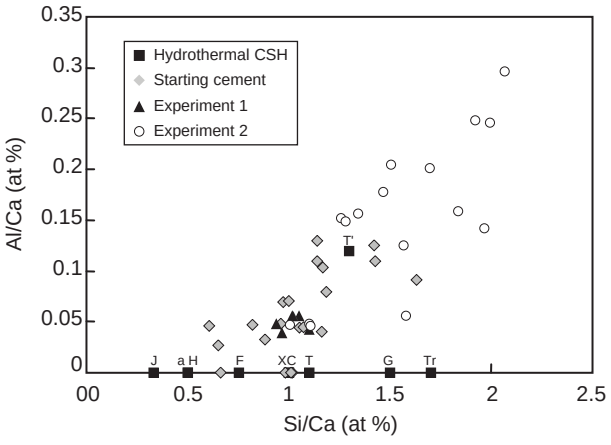

Figure 6

Al/Ca ratios plotted against Si/Ca ratios for individual C-S-H analyses. J: jaffeite (tricalcium silicate hydrate); a: alpha-C_2S hydrate; H: hillebrandite; F: foshagite; X: xonotlite; C: CSH(I); T: 11 Å tobermorite; G: gyrolite; Tr: truscottite; T': anomalous 11 Å tobermorite.

The composition data of hydrothermal CSH are from Taylor (1990) and St John *et al.* (1998).

individual microanalyses of the C-S-H show a small amount of Al. The microanalyses are reported in the Al/Ca *vs* Si/Ca plot of the Figure 6. The Si/Ca and Al/Ca atomic ratios vary from 1 to 2 and from 0.05 to 0.3 respectively. The spreading of composition is larger than in the experiment 1. The compositions are located on a trend and dispersed essentially above the position of the anomalous 11 Å tobermorite. The deduced mean composition of the C-S-H is presented in the Table 2. It shows an enrichment in Si and Al and a depletion in Ca relative to the experiment 1 and can be identified with the anomalous 11 Å tobermorite (Tob2) described by Taylor (1997) *(Table 2).*

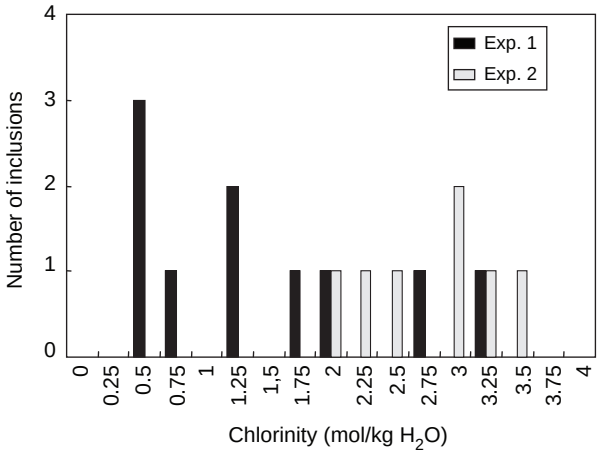

Figure 7

Histogram of chlorinities measured on the fluid inclusions of the experiment 1 (Exp. 1) and the experiment 2 (Exp. 2).

Fluids

Residual Gaseous Products

After the experiment 2, $n2_T$ was calculated using the Equation (2) with RP = 1.515 bar and V' = 72 cm^3. As $n2_T - n1_T$ is greater than 0 ($n2_T = 4.5 \times 10^{-3}$ and $n1_T = 5 \times 10^{-3}$ mol), then gas was consumed during the experiment. A total gas consumption rate *(GC_T)* of 10% has been calculated from the Equation (3). The Raman analysis performed on the residual gas gives a composition of 68.4% molar of H_2S and 31.6% molar of CO_2 *(Table 1).* Traces of H_2 have been also detected. This composition is close to the initial one *(Table 1).* Knowing $X1_{H_2S}$ (0.66) and $X1_{CO_2}$ (0.34) *(Table 1)* and $n1_T$, $n1_{H_2S}$ and $n1_{CO_2}$ are respectively 3.3×10^{-3} and 1.7×10^{-3} mol. Knowing $X2_{H_2S}$ (0.684) and $X2_{CO_2}$ (0.316) *(Table 1)* and $n2_T$, $n2_{H_2S}$ and $n2_{CO_2}$ are respectively 3.1×10^{-3} and 1.4×10^{-3} mol. These data allowed to determine the values of GC_{H_2S} and GC_{CO_2} from the Equation (5). They are respectively 6% and 16%.

Synthetic Fluid Inclusions

Two types of inclusions have been identified at room temperature:

– diphasic (liquid phase and vapour phase) *(Fig. 4, L)*;
– monophasic (liquid phase).

The diphasic inclusions are more numerous than the monophasic ones. At 200°C, both type of inclusions is monophasic (liquid phase). That means the fluid in the vicinity of the cement is an aqueous monophasic liquid under experimental conditions. 7 inclusions have been analysed by Raman microspectroscopy to determine the aqueous species and the chlorinity of the aqueous liquid phase. The measured chlorinities range from 2.1 to 3.7 molal *(Fig. 7).* There is no relation between the number of phases (1 or 2) and the amount of chlorine. The Figure 8 shows an example of Raman spectrum of an aqueous liquid phase at room temperature. HS^- is the major sulphur species and $H_2S_{(aq)}$ is present in small amount for the 7 inclusions. Eh-pH stability fields for the S-H_2O system at 200°C was calculated using CHESS program (Van der Lee and De Windt, 2002). The predominance of HS^- in water attests to basic conditions (8 < pH < 9) and low Eh conditions (–0.7 V< Eh < –0.5 V) at 200°C. No aqueous carbon species have been detected. The Raman analysis of the gaseous phases at room conditions of the biphasic inclusions detected only H_2S and sometimes traces of H_2.

2.4 Discussion

The mineralogy of the starting cement (SC) and of the characteristics of the starting brine (ionic species, chlorinity and pH) are exposed in the Table 3. Mineral transformation of the cement and the liquid evolution occurred during the two experiments are also exposed in the Table 3.

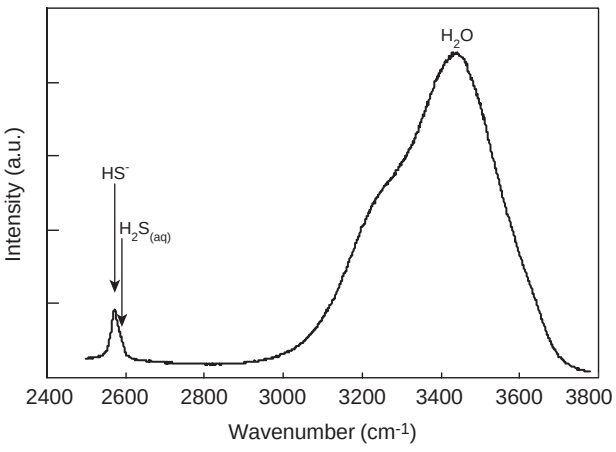

Figure 8

Raman spectrum of the liquid phase performed at room temperature on the inclusion of the micrograph L of the Figure 4.

TABLE 3

Bulk mineralogical changes of the cement and of the solution occurred during the experiments 1 and 2

	CEMENT					SOLUTION		
	Major phases	Minor phases				Ionic species	Chlorinity (molal)	pH
Starting	Tob1	Quartz	C_2S	C_4AF	Hgt1	Na^+, $C1^-$	2.75	10.3-11.2
Experiment 1 (without gas)	Xon	Dissolved	C-S-H	Fe oxides, Hgt2	Hgt2	Na^+, $C1^-$	0.5-3.5	Same as above
Experiment 2 (with gas)	Tob2, calcite	Residual	C-S-H	Pyrite	n.i.	Na^+, $C1^-$, HS^-, $H_2S_{(aq)}$	2.1-3.7	8.0-9.0

n.i.: non identified.

Tob1: $Ca_{5.4}\,Si_{5.5}\,Al_{0.4}\,O_{16}\,(OH)_2 \cdot 4\,H_2O$; Xon: $Ca_{5.8}\,Si_{5.9}\,Al_{0.3}\,O_{17}\,(OH)_2$; Tob2: $Ca_4\,Si_{6.1}\,Al_{0.5}\,O_{16}\,(OH)_2 \cdot 4\,H_2O$.

In the experiment 1 (without gas), the cement can be identified with aluminous xonotlite (Xon) *(Table 3)*. The main reaction occurred within the system is the transformation of Tob1 into Xon. The quartz was also fully dissolved probably by high pH conditions, explaining the rare large fluid inclusions sealing. We suppose the pH of the experiment 1 to be close to the starting values (10.3-11.2) since the solution is in equilibrium with C-S-H. C_2S have been probably hydrated to form Xon. The pink colour of the reacted cement could be attributed to the presence of iron (hydr)oxides. These oxides as well as part of newly formed hydrogarnet phases (Hgt2) probably formed from the initial C_4AF (Taylor, 1997). The reaction describing these bulk mineralogical transformations can be written as follows:

$$\text{Tob1} + 0.2\,C_2S + 0.2\,SiO_2 \Leftrightarrow \text{Xon} + 0.1\,Al(OH)_{3(aq)} + 4\,H_2O \quad (7)$$

This reaction shows a release of water while the Tob1 converts into Xon. This release of water could dilute the brine and could explain the decrease of salinity observed within the fluid inclusions. The C_4AF, Hgt1, Fe oxides and Hgt2 are not represented in the reaction. These minerals control the balance of the minor elements Fe and Al in the cement.

In the experiment 2 (with gas), the initial tobermorite (Tob1) have been converted into anomalous tobermorite (Tob2) with a depletion in Ca *(Table 3)*. The released Ca was combined with carbon aqueous species to form calcite. The basic character of the interstitial solution ($8 < pH < 9$) leads to the partial dissolution of the quartz. The iron and sulphur contained in the pyrites are provided respectively by the C_4AF and the H_2S. However, the H_2S consumption is essentially attributed to the sulphidation of steel (not presented in this paper). The Reaction (8) illustrates these bulk mineralogical transformations:

$$\text{Tob1} + 0.1\,C_4AF + 0.6\,SiO_2 + 0.6\,H_2S + 1.6\,CO_2 + 0.2\,Fe^0 \Leftrightarrow \text{Tob2} + 1.6\,CaCO_3 + 0.1\,FeS_2 + 0.2\,H_2 \quad (8)$$

In the Reaction (8), the molar coefficients of H_2S and CO_2 (respectively 0.6 and 1.6) are in agreement with the GC_{H_2S} to GC_{CO_2} ratio (0.375). The Fe^0 is provided by the steel. The C_2S are not represented in this reaction but can also contribute to Tob2 formation. The Reaction (8) predicts the formation of 1.6 mol of calcite plus 1 mol of Tob2 from 1 mol of Tob1. In terms of volume, that means the reacted cement contains 5 times more tobermorite than calcite. This ratio is coherent with the observation of the Figure 4, H. The reaction of C-S-H with carbon dioxide producing calcite and C-S-H with higher Si/Ca ratio is referred as carbonation of cement. The carbonation process is known to decrease the pH of the interstitial solution (Taylor, 1997; St John *et al.*, 1998). Such pH decrease is observed during the experiment 2 from the range 10.3-11 to the range 8-9. In the experimental conditions, limited to 15 days, the carbonation is not complete since it produced residual C-S-H and no amorphous silica. The presence of the H_2S-CO_2 mixture (experiment 2) induces carbonation of the cement and sulphidation of iron bearing phases (steel and C_4AF) coupled with a pH and Eh decrease. Such conditions prevent the formation of xonotlite in brine environment (experiment 1).

CONCLUSION

The described experimental procedure has been specially designed to study the H_2S+CO_2-(hydrocarbons)-brine-well(rocks) interactions that occur at reservoirs-well interfaces of sour gas geological storage. This procedure is appropriate to study different solid-liquid-gas systems at geologically-relevant P-T (up to 990 bar and 450°C). High gas concentrations can be reached with respect to safety rules. By example, effects of dry supercritical H_2S+CO_2 or pure CO_2 on solids reactivity can be examined. The initial gas concentration of the system is controlled accurately. After hydrothermal experiments, mass balances of gases can be calculated. The technique of synthetic fluid inclusions as fluid sampling method is included in the analysis protocol. It allows to determine the state and the speciation of the fluid phases at experimental conditions.

Two experiments have been conducted to show the application of this procedure to well cement aging. The reactants of the experiment 1 were cement+steel+brine while the reactants of the experiment 2 were cement + steel + brine + H_2S + CO_2. Without gas, the initial cement is converted to an assemblage of xonotlite while the presence of gas causes the formation of calcite around the cement and the formation of pyrites within the cement and around the steel. The calculated gas mass balance allowed to estimate the volume amount of newly formed minerals.

The results acquired using this experimental procedure give the input data and strong constraints for numerical modelling. For this purpose, the quantification of the starting and reacted mineral phases will be improved. Additional parameters such as the ionic fluid composition are essential to conduct numerical percolation simulations. The ionic composition of the aqueous phase trapped in inclusions will be further determined by laser ablation coupled with ICP-MS (ion coupled plasma-mass spectrometry) (Audétat *et al*., 2000) or LIBS (laser induced breakdown spectroscopy) (Fabre *et al*., 1999; Fabre *et al*., 2002;). The petrophysical properties of the cement such as the porosity changes are also an important parameter for the prediction of durability. The development of techniques for the determination of that parameter is thus essential.

AKNOWLEDGEMENTS

This project is supported by *Total*. The authors gratefully thank Jean-Claude Lacharpagne of *Total* who initiated this research project. We thank also Gilles Bessaques and Alain Rouiller for their technical support during apparatus making, Régine Mosser-Ruck for XRD analyses, Alain Kohler and Jaffar Ghambaja of *Service commun de l'université H.-Poincaré* for SEM and TEM analyses and Thérèse Lhomme for Raman investigations.

REFERENCES

Albarran, J.L., Martinez, L., and Lopez, H.F. (1999) Effect of heat treatment on the stress corrosion resistance of a microalloyed pipeline steel. *Corrosion Science*, **41**, 1037-1049.

Audétat, A., Günter, D., and Heinrich, C.A. (2000) Causes for large-scale metal zonation around mineralized plutons: fluid inclusion LA-ICP-MS evidence from the Mole granite, Australia. *Economic Geology*, **95**, 1563-1581.

Bachu, S. (2000) Sequestration of CO_2 in geological media: criteria and approach for site selection in response to climate change. *Energy Conversion and Management*, **41,** 953-970.

Bachu, S. (2002) Sequestration of CO_2 in geological media in response to climate change: road map for site selection using the transform of the geological space into the CO_2 phase space. *Energy Conversion and Management*, **43**, 87-102.

Bodnar, R.J. and Sterner, S.M. (1987) Synthetic fluid inclusions. In: *Hydrothermal Experimental Techniques* (ed. Ulmer, G.C. and Barnes, H.L.), 423-457. John Wiley & sons.

Bruant, R.G.J., Guswa, A.J., Celia, M.A., and Peters, C.A. (2002) Safe storage of CO_2 in deep saline aquifers. *Environmental Science & Technology*, **36,** 11, 241 A-245 A.

Carneiro, R.A., Ratnapuli, R.C., and Freitas Cunha Lins, V. (2003) The influence of chemical composition and microstructure of API linepipe steels on hydrogen cracking and sulfide stress corrosion cracking. *Materials Science and Engineering*, **A357**, 104-110.

Carroll, J.J. and Maddocks, J.R. (1999) Design considerations for acid gas injection. *Laurance Reid Gas Conditionning Conference. http://www.gasliquids.com/papers/lrgcc99.pdf*

Celia, M.A. and Bachu, S. (2002) Geological sequestration of CO_2: is leakage unavoidable and acceptable? *GHGT-6, 6th Int. conf. on GreenHouse Gas control Technologies). http://www.princeton.edu/~cmi/research/kyoto02/celia&bachu.kyoto%2002.pdf*

Chakma, A. (1997) Acid gas re-injection - a practical way to eliminate CO_2 emmissions from gas processing plants. *Energy Conversion and Management*, **38,** (Supplt), S 205-S 209.

Cieslak, J., Dubiel, S.M., and Zurek, Z. (1998) Investigation of scales resulted from a high-temperature sulphidation of Fe-Cr alloys. *Journal of Alloys and Compounds*, **26**, 297-304.

Clavel, T., Falcy, M., Hesbert, A., Jargot, D., Protois, J.C., Reynier, M., and Schneider, O. (1997) Sulfure d'hydrogène. *Fiche toxicologique n° 32 de l'INRS. http://www.inrs.fr/*

Connock, L. (2001) Acid gas re-injection reduces sulphur burden. Sulphur, **272**, 35-41.

Cui, Z.D., Wu, S.L., Li, C.F., Zhu, S.L., and Yang, X.J. (2004) Corrosion behaviour of oil tube steels under conditions of multiphase flow saturated with super-critical carbon dioxide. *Materials Letters*, **58**, 1035-1040.

Davison, J., Freund, P., and Smith, A. (2001). Putting carbon back into the ground. *IEA Greenhouse Gas R&D Programme Report. http://www.ieagreen.org.uk/putcback.pdf*

Domizzi, G., Anteri, G., and Ovejero-Garcia, J. (2001) Influence of sulphur content and inclusion distribution on the hydrogen induced blister in pressure vessel and pipeline steels. *Corrosion Science*, **43**, 325-339.

Dubessy, J., Poty, B., and Ramboz, C. (1989) Advances in C-O-H-N-S fluid geochemistry based on Raman analysis of fluid inclusions. *European Journal of Mineralogy*, **1**, 517-534.

Dubessy, J., Buschaert, S., Lamb, W., and Pironon, J. (2001) Methane-bearing aqueous fluid inclusions: Raman analysis, thermodynamic modelling and application to petroleum basins. *Chemical Geology*, **173**, 193-205.

Dubessy, J., Lhomme, T., Boiron, M.C., and Rull, F. (2002) Determination of chlorinity in aqueous fluids using Raman spectroscopy of the stretching band of water at room temperature: application to fluid inclusions. *Applied Spectroscopy*, **56**, 99-106.

Fabre, C., Boiron, M.C., Dubessy, J., and Moissette, A. (1999) Determination of ions in individual fluid inclusions by laser ablation - optical emission spectroscopy: development and applications to natural fluid inclusions. *Journal of Analytical Atomic Spectrometry*, **14**, 913-922.

Fabre, C., Boiron, M.C., Dubessy, J., Cathelineau, M., and Banks, D. (2002) Palaeo-fluid chemistry of single fluid event: a bulk and in-situ multi-technique analysis (LIBS, Raman) of an alpine fluid (Mont-Blanc). *Chemical geology*, **182**, 249-262.

Feugier, A. (2002) Une réponse à l'effet de serre: la séquestration du CO_2. *Lettre de la Direction générale de l'Énergie et des Matières Premières*, **20**, 3-8.

Frantz, J.D., Zhang, Y., Hickmott, D.D., and Hoering, T.C. (1989) Hydrothermal reactions involving equilibrium between minerals and mixed volatiles. 1. Techniques for experimentally loading and analysing gases and their application to synthetic fluid inclusions. *Chemical Geology*, **76**, 57-70.

Frantz, J.D., Popp, R.K., and Hoering, T.C. (1992) The compositional limits of fluid immiscibility in the system H_2O-NaCl-CO_2 as determined with the use of synthetic inclusions in conjunction with mass spectrometry. *Chemical Geology*, **98**, 237-255.

Giammar, D.E., Myneni, S.C.B., Bruant, R.G., and Peters, C.A. (2002). Characterization of mineral surfaces weathered under high pressure and carbon dioxide conditions. *Research Presentation. Carbon Mitigation Initiative (CMI) Group,* Princeton Environmental Institute. *http://www.princeton.edu/~cmi/research/Storage/Presentations/characterization%20of%20mineral.pdf*

Gravier, J.F. (1986) *Propriétés des fluides de gisements. Cours de production - tome 2,* Institut français du pétrole.

Guillaume, D., Teinturier, S., Dubessy, J., and Pironon, J. (2003) Calibration of methane analysis by Raman spectroscopy in H_2O-NaCl-CH_4 fluid inclusions. *Chemical Geology*, **14103**, 1-9.

Gunter, W.D., Wiwchar, B., and Perkins, H. (1997) Aquifer disposal of CO_2-rich greenhouse gases: extension of the time scale of experiment for CO_2-sequestring reactions by geochemical modelling. *Mineralogy and Petrology*, **59**, 121-140.

IPCC (2001) Climate Change 2001: The Scientific Basis. Contribution of Working Group I to the Third Assessment Report of the Intergovernmental Panel on Climate Change. *IPCC Report. http://www.ipcc.ch/pub/spm22-01.pdf*

Jahn, F., Cook, M., and Graham, M. (1998) *Hydrocarbon Exploration and Production*. Elsevier.

Kalousek, G.L. (1957) Crystal chemistry of hydrous calcium silicates: I, substitution of aluminum in lattice of tobermorite. *Journal of the American Ceramic Society*, **40,** 3, 74-80.

Kaszuba, J.P., Janecky, D.R., and Snow, M. G. (2003) Carbon dioxide reaction processes in a model brine aquifer at 200 °C and 200 bars: implications for geologic sequestration of carbon. *Applied Geochemistry*, **18**, 1065-1080.

Krilov, Z., Loncaric, B., and Miksa, Z. (2000) Investigation of a long-term cement deterioration under a high-temperature, sour gas downhole environment. *Society of Petroleum Engineers Journal, Paper SPE 58771.*

Lamb, W.M., Popp, R.K., and Boockoff, L.A. (1996) The determination of phase relations in the CH_4 - H_2O - NaCl system at 1 kbar, 400 to 600°C using synthetic fluid inclusions. *Geochimica et Cosmochimica Acta*, **60,** 11, 1885-1897.

Lamb, W.M., Mcshane, C.J., and Popp, R.K. (2002) Phase relations in the CH_4-H_2O-NaCl system at 2 kbar, 300 to 600°C as determined using synthetic fluid inclusions. *Geochimica et Cosmochimica Acta*, **22**, 3971-3986.

Landais, P., Michels, R., and Poty, B. (1989) Pyrolysis of organic matter in cold-seal pressure autoclaves. Experimental approach and applications. *Journal of Analytical and Applied Pyrolysis*, **16**, 103-115.

Méducin, F., Noïk, C, Rivereau, A., Hamel, G. and Zanni, H. (2001) Oilwell cements: NMR contribution to establish the phase diagram pressure/temperature of the mixture H_2O/Ca_3SiO_5. *Comptes Rendus de l'Académie des Sciences de Paris/Chemistry* **4**, 801-804.

Méducin, F., Noïk, C, Rivereau, A. and Zanni, H. (2002) Complementary analyses of a tricalcium silicate sample hydrated at high pressure and temperature. *Cement and Concrete Research*, **32**, 65-70.

Mindat.org (2004). *http://www.mindat.org/index.php*

Onan, D.D. (1984) Effects of supercritical carbon dioxide on well cements. *Society of Petroleum Engineers Journal, Paper SPE 12593.*

Pearce, J.M., Holloway, S., Wacker, H., Nelis, M.K., Rochelle, C., and Bateman, K. (1996) Natural occurences as analogues for the geological disposal of carbon dioxide. *Energy Conversion and Management*, **37,** 6-8, 1123-11128.

Rasband, W. (2004) *ImageJ 1.32 h.* National Institute of Health, USA. *http://rsb.info.nih.gov/ij/*

Reeve, D.A. (2001) Le captage et le stockage des émissions de dioxyde de carbone. Un outil précieux pour le Canada dans le contexte du Protocole de Kyoto. *Rapport du Bureau de Recherche et de développement énergétiques, ressources naturelles,* Canada. *http://www2.nrcan.gc.ca/es/oerd/CMFiles/kyotoFrench225LOU-1022002-9476.pdf*

Seyfried, W.E.J., Janecky, D.R., and Berndt, M.E. (1987) Rocking autoclaves for hydrothermal experiments. The flexible reaction-cell system. In: *Hydrothermal Experimental Techniques* (ed. Ulmer, G.C. and Barnes, H.L.), 216-239, John Wiley & Sons.

Shen, J.C. (1989) Effects of CO_2 attack on cement in high-temperature. *Society of Petroleum Engineers Journal, Paper SPE/IADC 18618.*

Shiraki, R. and Dunn, T.L. (2000) Experimental study on water-rock interactions during CO_2 flooding in the Tensleep Formation, Wyoming, USA. *Applied Geochemistry*, **15**, 265-279.

Soong, Y., Goodman, A L., McCarthy-Jones, J.R., and Baltrus, J.P. (2004) Experimental and simulation studies on mineral trapping of CO_2 with brine. *Energy Conversion and Management*, **45,** 11-12, 1845-1859.

St John, D.A., Poole, A.B., and Sims, I. (1998) *Concrete Petrography*. Arnold.

Taylor, H.F.W. (1997) *Cement Chemistry*. Thomas Telford.

Teinturier, S. (2002) Diagénèse expérimentale du quartz en présence d'hydrocarbures. *PhD Thesis/Thèse*, université de Nancy I.

Teinturier, S., Elie, M., and Pironon, J. (2003) Evidence of oil cracking using synthetic petroleum inclusion. *Journal of Geochemical Exploration*, **78-79**, 421-425.

Teinturier, S. and Pironon, J. (2003) Synthetic fluid inclusions as recorders of microfracture healing and overgrowth rates. *American Mineralogist*, **88**, 1204-1208

Van der Lee, J. and De Windt, L. (2002) *CHESS Tutorial and Cookbook. Updated for version 3.0. Users Manual Nr LHM/RD/02/13*, École des mines de Paris, Fontainebleau, France.

Webmineral.com (2004) *http://www.webmineral.com/*

Wichert, E. (1996) Sulfur disposal by acid gas injection. *Society of Petroleum Engineers Journal, Paper SPE 35585*, 193-200.

Wichert, E. (1997) Acid gas injection eliminates sulfur recovery expense. *Oil and Gas Journal*, **95,** 16, 64-72.

Final manuscript received in November 2004